JOURNAL OF Materials Chemistry

A mixed valent iron oxycarbonate closely related to the $n=3$ member of the RP series $Sr_4Fe_{3-x}(CO_3)_xO_{10-4x-\delta}$

Yohann Bréard, Claude Michel,* Maryvonne Hervieu and Bernard Raveau

Laboratoire CRISMAT, UMR6508-CNRS, ISMRA et Université de Caen, 6, Boulevard du Maréchal Juin, 14050 Caen Cédex, France; E-mail: claude.michel@ismra.fr

Received 31st January 2000, Accepted 7th March 2000

A new oxycarbonate $Sr_4Fe_{2.6}O_{8.2}(CO_3)_{0.4}$ closely related to the $n=3$ member of the Ruddlesden–Popper family has been synthesized; it exhibits the presence of Fe^{3+} and Fe^{4+} in low spin configuration and a magnetic transition at 35 K.

Layered oxides of the Ruddlesden and Popper (RP) family[1] have been extensively investigated for the generation of new physical properties with potential applications such as superconductivity at high temperature in cuprates[2] or colossal magnetoresistance (CMR) in manganites.[3] The possibility to substitute carbonate groups for copper in these structural types allowed numerous copper oxycarbonates involving bismuth, thallium or mercury to be synthesized.[4] In contrast to copper, manganese does not show such an aptitude to form layered oxycarbonates, though one oxycarbonate with a tunnel structure, $Sr_5Mn_4O_{10}(CO_3)$, has been synthesized.[5]

Among the various transition elements, iron is a very attractive candidate for the creation of layered oxycarbonates. Parent iron oxides closely related to the RP phases were indeed previously isolated as shown for the oxides $Sr_4Fe_3O_{10}$[6] and $(Tl,Pb)_1Sr_4Fe_2O_{9-\delta}$.[7,8] Moreover, iron has the advantage that it can exhibit several oxidation states, especially Fe(III) and Fe(IV) which may induce original magnetic and transport properties. For this reason we have investigated the possibility to introduce carbonate groups in the Sr–Fe–O system. Here we report a new mixed valent iron oxycarbonate $Sr_4Fe_{3-x}(CO_3)_xO_{10-4x-\delta}$, with $x=0.4$, which corresponds to the substitution of CO_3 groups for FeO_6 octahedra in the $n=3$ member of the RP phase $Sr_4Fe_3O_{10}$. This oxide is characterized by a magnetic transition at 35 K.

In order to introduce CO_3 groups in the framework of such oxides, we have studied the reaction between SrO_2 containing 10 mol% $SrCO_3$ (Aldrich) and Fe_2O_3, working in a sealed evacuated ampoule in order to avoid CO_2 departure. The compounds were intimately mixed, pressed in the form of bars and heated in silica tubes up to 1200 °C for 12 h. The heating and cooling down to room temperature were performed in 6 h. For these experimental conditions, a single phase could be obtained, starting from a mixture of 4.6 "SrO_2" + 1.5 Fe_2O_3. The EDX analysis of numerous crystallites revealed the cationic formula $Sr_4Fe_{2.6}$, in perfect agreement with the nominal composition. The mean oxidation state of iron, determined by redox titration, was +3.55 leading to an oxygen stoichiometry close to 8.2 per formula unit, *i.e.* close to the expected value (8.4).

The ED study was carried out with a JEOL 200CX microscope, tilting around the crystallographic axes. The system of intense Bragg reflections is characteristic of an I-type tetragonal cell, with $a\approx3.85$ Å and $c\approx28$ Å (Fig. 1a). On this basis, the XRPD pattern, registered with a Philips vertical diffractometer equipped with a secondary graphite monochromator (Cu-Kα radiation), can be well indexed in a tetragonal cell (space group *I4/mmm*) with lattice constants: $a=b=3.8668(1)$ Å, $c=28.161(1)$ Å. These cell parameters and conditions of reflection (*hkl*: $h+k+l=2n$) are consistent with those expected for an $n=3$ member of the RP series. A part of the crystallites exhibit however extra weak reflections which either violate the I-type conditions or attest to the existence of local superstructures. The high resolution electron microscopy (HREM) study was carried out with a TOPCON 002B microscope (point resolution: 1.8 Å). The HREM images recorded along [100] confirm the layer stacking mode: the structure is built up from two adjacent [SrO] layers, forming one rock salt-type layer, intergrown along ***c*** with a triple perovskite slice. This is illustrated in Fig. 1b, where the high electron density zones appear as the darker dots. The contrast observed on the thin crystal edges is characteristic of the presence of carbonate groups substituting the Fe polyhedra within the intermediate layer of the triple perovskite slice. Such

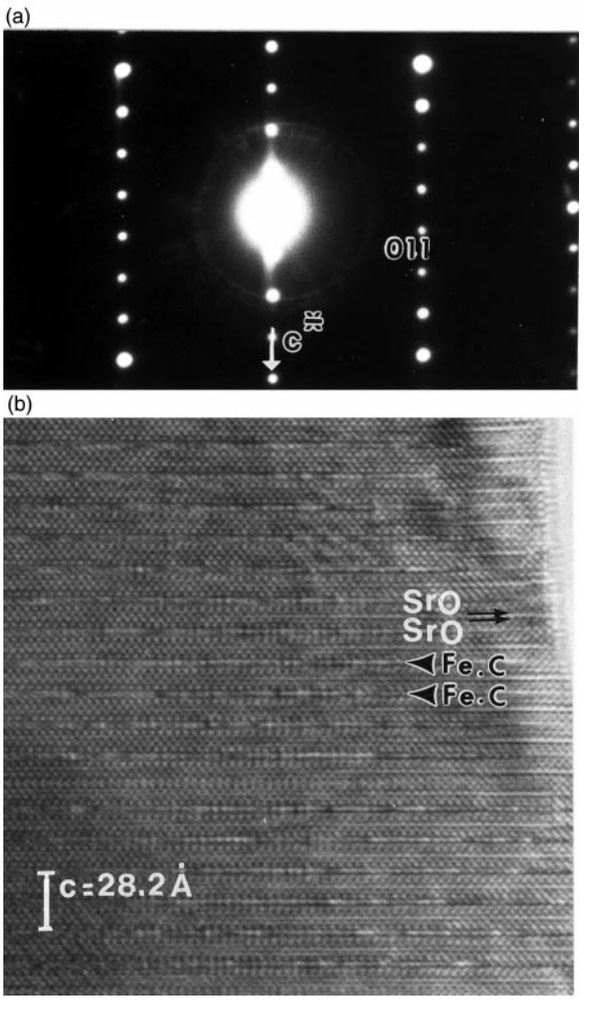

Fig. 1 a) [100] ED pattern and b) HREM image of $Sr_4Fe_{2.6}O_{8.2}(CO_3)_{0.4}$.

DOI: 10.1039/b000814l

an effect can indeed be compared to that observed in the 123-type oxycarbonate[9] or the Tl(Hg,Bi) superconducting cuprates.[10] The uneven contrast observed at the level of the intermediate layer (see arrow Fe,C in Fig. 1b) suggests an average structure with a random distribution of Fe and C species.

For the structure determination, neutron diffraction data were collected at room temperature on the 3T2 diffractometer at the Laboratoire Léon Brillouin (Saclay, France), with $\lambda = 1.2251$ Å. ND data were treated using Rietveld profile analysis (FULLPROF program[11]), the scattering lengths of elements were those included in the program package.

Lattice constants were first refined ($a = 3.8650(1)$ Å, $c = 28.137(1)$ Å). *I*4/*mmm* was used as the space group. The starting model was that of a classical $n = 3$ member of the RP family with 40% of carbon occupying the iron site (Fe(2)) in the intermediate layer. Considering our previous studies on copper oxycarbonates,[12] which showed the CO_3 triangles approximately parallel to ***c***, a supplementary oxygen (O(5)), lying about 1.3 Å from carbon, was introduced in the Fe(2)–C plane with content fixed to be equal to that of C. The number of Fe(2) equatorial oxygen atoms (O(4)) was first reduced from the same amount. In these conditions, positional parameters and isotropic thermal factors were refined, leading to $R_p = 7.3\%$, $R_{wp} = 10.1\%$, $R_{Bragg} = 12.5\%$, but for high B values for the oxygen atoms surrounding Fe(2) sites (O(1), $B = 3$ Å^2, and O(4), $B = 2.4$ Å^2). A supplementary 'apical' oxygen atom (O′(1)) was considered, it was assumed to be linked only to carbon at a distance close to 1.3 Å, whereas O(1) was assumed to be linked only to Fe(2). With this model , the value of the O′(1)–C–O′(1) angle is 180°, very different from that expected in a CO_3 group; this value can be reduced considering a displacement in the *ab* plane from the initial position $x = y = 0$. Oxygen atoms lying in the carbon–iron plane (O(4) and O(5)) were disordered over more general positions. Final refinement, including the oxygen number around Fe(2), allowed $R_p = 5.6\%$, $R_{wp} = 7.5\%$, $R_{Bragg} = 6.9\%$ for the values of the variable parameters listed in Table 1. The experimental, calculated and difference powder neutron diffraction pattern are plotted in Fig. 2. Calculated interatomic distances are given in Table 2.

The chemical composition issued from refinement is $Sr_4Fe_{2.62}O_{8.18}(CO_3)_{0.38}$, *i.e.* very close to that deduced from EDX and chemical analyses. The schematic view of the structure shows that this phase can be described as intermediate between two limiting structures, $Sr_4Fe_3O_{10}$ and $Sr_4Fe_2CO_3O_6$. The synthesis of $Sr_4Fe_2CO_3O_6$, with $a = 3.8875(1)$ Å, $c = 27.997(1)$ Å, by heating the mixture '$SrCO_3$–3SrO–Fe_2O_3' in an evacuated ampoule confirms this view point (Fig. 3). The Sr–O distances are close to those usually observed. Iron atoms in the two external perovskite layers (Fe(1)) are either in distorted octahedra with one short and one long apical bond

Table 1 Refined parameters from neutron diffraction data for $Sr_4Fe_{2.6}O_{8.2}(CO_3)_{0.4}$[a]

Atom	Site	x	y	z	B/Å^2	n
Sr(1)	4*e*	0.0	0.0	0.5717(13)	0.89(5)	4
Sr(2)	4*e*	0.0	0.0	0.70156(9)	0.60(5)	4
Fe(1)	4*e*	0.0	0.0	0.14192(8)	0.40(3)	4
Fe(2)	2*a*	0.0	0.0	0.0	1.12(6)[b]	1.24(5)
C	2*a*	0.0	0.0	0.0	1.12(6)[b]	0.76(5)
O(1)	4*e*	0.0	0.0	0.0698(3)	0.6(2)[c]	2.00(6)
O′(1)	16*n*	0.0	0.938(4)	0.0496(5)	0.6(2)[c]	1.52(5)
O(2)	4*e*	0.0	0.0	0.2103(1)	0.82(2)	4
O(3)	8g	0.0	0.5	0.63534(9)	0.88(4)	8
O(4)	16*n*	0.0	0.454(4)	0.498(2)	1.5(4)	2.37(10)
O(5)	16*n*	0.0	0.31(2)	0.010(2)	3.5(1)	0.76(5)

[a]Constraints: n[C] + n[Fe(2)] = 1, n[O′(1)] = 2n[C] = 2n[O(5)]. [b]Constrained to have the same value. [c]Constrained to have the same value.

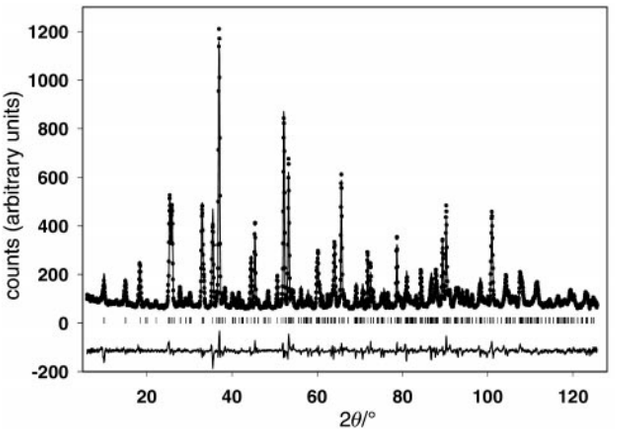

Fig. 2 Experimental (dots), calculated and difference (solid lines) powder neutron diffraction patterns for $Sr_4Fe_{2.6}O_{8.2}(CO_3)_{0.4}$. Vertical bars show the Bragg angle positions.

Table 2 Calculated interatomic distances

M–O	$\times n$[a]	d/Å	M–O	$\times n$[a]	d/Å
Sr(1)–O(1)	2	2.734(1)	Fe(1)–O(1)	0.5	2.030(9)
–O′(1)	0.8	2.64(1)	–O′(1)	0.4	2.61(1)
–O′(1)	0.8	2.97(1)	–O(2)	1	1.925(3)
–O(3)	4	2.633(3)	–O(3)	4	1.941(1)
–O(4)	1	2.64(5)			
–O(4)	1	2.71(4)	Fe(2)–O(1)	1.7	1.964(9)
–O(4)	1	2.88(5)	–O(4)	3.8	1.941(2)
–O(4)	1	2.96(5)			
–O(5)		2.69(4)	C–O′(1)	2	1.41(1)
			–O(5)	1	1.23(6)
Sr(2)–O(2)	1	2.479(4)			
–O(2)	4	2.744(1)			
–O(3)	4	2.685(2)			

[a]Number of neighbours, taking into account site occupancies.

distances when linked to Fe(2) or in square pyramids when linked to C, considering that oxygen at 2.61 Å does not participate in the Fe(1) polyhedra. It should be noted that this description does not take into account some oxygen vacancies observed on O(1) sites (2.00 atoms instead of 2.48). The Fe(2)–

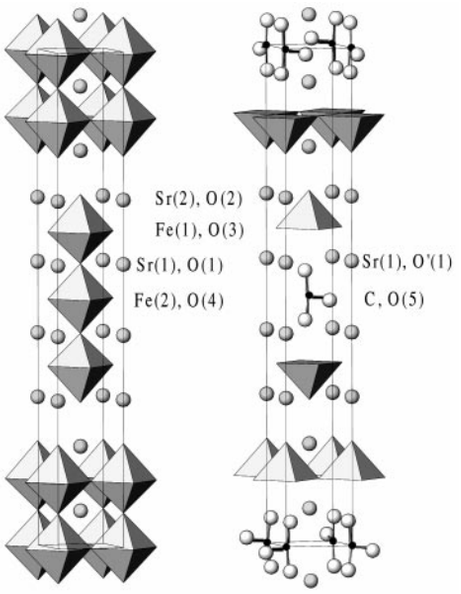

Fig. 3 The structure can be considered as a "mixture" of two limiting structures: $Sr_4Fe_3O_{10}$ (left) and $Sr_4Fe_2O_6CO_3$ (right). In the latter, different possible orientations of the carbonate groups are shown.

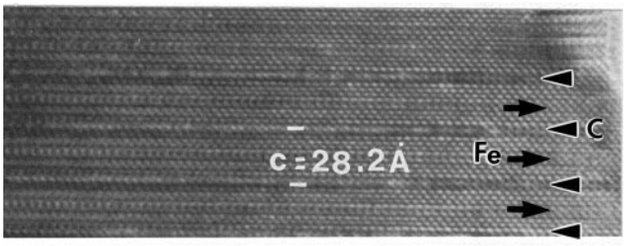

Fig. 4 [100] HREM image showing the local stabilization of the member $[Sr_4Fe_3O_{10}]_1$ $[Sr_4Fe_2(CO_3)O_6]_1$.

O polyhedra are slightly elongated octahedra with some oxygen vacancies both on apical and equatorial oxygen positions. The latter are probably the consequence of the presence of carbon on the Fe(2) site, which exhibits a different environment. Carbon atoms are surrounded by 3 oxygen atoms forming a distorted triangle with O–C–O angles of 158(1)° for O′(1)–C–O′(1), 115(3)° and 87(3)° for O′(1)–C–O(5) and bond distances ranging from 1.23 to 1.41 Å. The isotropic thermal factors for the oxygens surrounding carbon remain rather high. The probable reason for this is that the CO_3 groups, which are parallel to ***c***, can more or less freely rotate in the *ab* plane whereas in our model their orientation is only parallel to ***a*** or ***b***.

This structural study leads to a model which supposes a statistical distribution of the carbonate groups in the intermediate layer, in agreement with the irregular contrast observed at that level in HREM images (Fig. 1b). However, in most of the crystallites, local ordering is observed which generates the aforementioned weak extra reflections in the ED patterns. They result from the ordering of carbonate groups and Fe polyhedra, which exhibit various and complex relative arrangements. One example is given in Fig. 4 which presents a local sequence of one C-rich and one Fe-rich layer regularly stacked along ***c***. It corresponds to the regular intergrowth of two limiting members $Sr_4Fe_3O_{10}$ and $Sr_4Fe_2CO_3O_6$ (Fig. 3). The *c* parameter remains constant but the symmetry is no longer I-type. Other local ordered domains have been detected, made of complex intergrowths, along [001] as the above example, but also along [100] of $Sr_4Fe_3O_{10}$ and $Sr_4Fe_2CO_3O_6$ structures should be stabilized.

The magnetic susceptibility measurements were performed in the range 4–400 K in an applied field of 3000 G using an AC–DC SQUID Quantum Design magnetometer (ZFC and FC method). The hysteresis between both curves indicates that some ferromagnetic interactions coexist with the antiferromagnetic ones below 35 K. This behavior is reminiscent of a spin-glass like state. A magnetic structure from neutron diffraction data collected at low *T* will be performed in order to clarify this point. For $T>100$ K, the linear part of χ^{-1} (inset Fig. 5), fitted with a Curie–Weiss law

$$\chi=\chi_0+\frac{c}{T-\theta_P}$$

where *C* is the Curie constant, θ_P the paramagnetic Curie temperature and χ_0 the temperature independent susceptibility, leads to a negative θ_P value (−25 K), typical of antiferromagnetic interactions and an effective magnetic moment of 2.25 μ_B per mol of Fe. Taking into account the ratio $Fe^{3+}/Fe^{4+}\approx 1$ the value of the effective magnetic moment could correspond to low spin configuration ($\mu_{eff}=2.34\ \mu_B$) for Fe^{3+} and Fe^{4+}.

The presence of mixed valence iron could induce transport properties. The electrical resistivity was measured from liquid helium temperature to 400 K by means of a Physical Properties

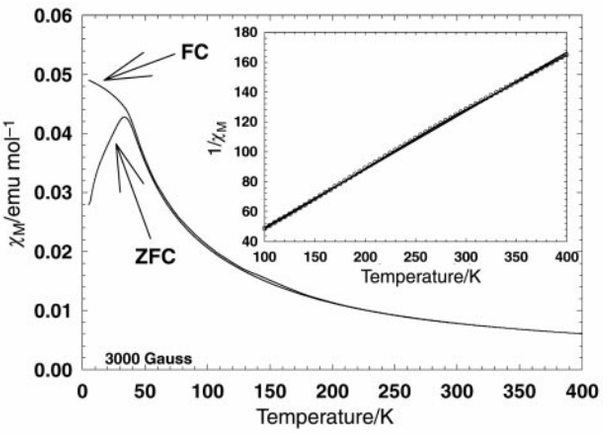

Fig. 5 $\chi_M(T)$ curves obtained from ZFC and FC $M(T)$ curves recorded in 3000 G. Inset: $\chi^{-1}(T)$ curve (open circles are experimental points whereas solid line is the fit).

Measurements System (PPMS) from Quantum Design (four probe method). A dramatic decrease of the resistivity from more than $10^6\ \Omega$ cm at 50 K to 2 Ω cm at 400 K is observed (below 50 K the resistivity is too high to be measured). The data were fitted with an Arrhenius law used for variable range hopping mechanism, $\rho=\rho_0\exp(A/T)^{1/n+1}$, where *n* is the dimensionality of the system. The best fit was obtained for $n=2$, in agreement with the bidimensional character of the structure. Measurements in a magnetic field of 7 T do not allow us to detect any magnetoresistance property.

Acknowledgements

The authors are grateful to Dr. Françoise Bourée and Mr. Bernard Rieu (Laboratoire Léon Brillouin, Saclay) for collection of neutron diffraction data.

Notes and references

1 R. S. Ruddlesden and P. Popper, *Acta Crystallogr.*, 1957, **10**, 538; R. S. Ruddlesden and P. Popper, *Acta Crystallogr.*, 1958, **11**, 54.
2 B. Raveau, C. Michel, M. Hervieu and D. Groult, *Crystal Chemistry of High T_c Superconducting Copper Oxides*, Springer Verlag, Berlin, 1991.
3 M. Imada, A. Fujimori and Y. Tokura, *Rev. Mod. Phys.*, 1999, **70**, 1039; see also *Colossal Magnetoresistance, Charge Ordering and Related Properties of Manganese Oxides*, ed. C. N. R. Rao and B. Raveau, World Scientific, Singapore, 1998.
4 B. Raveau, C. Michel, M. Hervieu and A. Maignan, *J. Mater. Chem.*, 1995, **5**, 803; B. Raveau, C. Michel, M. Hervieu and A. Maignan, *J. Alloys Compd.*, 1995, **229**, 134; C. N. R. Rao and B. Raveau, *Transition Metal Oxides*, VCH, Weinheim, 1995.
5 V. Caignaert, B. Domengès and B. Raveau, *J. Solid State Chem.*, 1995, **120**, 279.
6 C. Brisi and P. Rolando, *Ann. Chim. (Rome)*, 1969, **59**, 385.
7 N. Nguyen, Ph. Daniel, D. Groult and B. Raveau, *Mater. Chem. Phys.*, 1996, **45**, 33; and references therein.
8 T. Seguelong, P. Maestro, J. C. Grenier, L. Fournes and M. Pouchard, *Physica B*, 1995, **215**, 427.
9 Y. Miyasaki, H. Yamane and T. Hirai, *Physica C*, 1992, **199**, 53; B. Domengès, M. Hervieu and B. Raveau, *J. Solid. State Chem.*, 1993, **106**, 271.
10 M. Hervieu, G. Van Tendeloo, C. Michel, D. Pelloquin and B. Raveau, *Microsc. Microanal. Microstruct.*, 1996, **7**, 107.
11 J. R. Carvajal, *Collected Abstracts of a Powder Diffraction Meeting*, ed. J. Galy, Toulouse, France, 1990, p. 127.
12 S. Malo, C. Michel, D. Pelloquin, M. Hervieu, O. Toulemonde and B. Raveau, *Physica C*, 1998, **304**, 213.